

Hadron Production in Proton-Proton Scattering in NEXUS 3

F.M. Liu^{1,2,4*}, T. Pierog^{3,4}, J. Aichelin⁴, K. Werner⁴

10th November 2018

¹ Institute of Particle Physics, Central China Normal University, Wuhan, China.

² Institut fuer Theoretische Physik, JWG Frankfurt Universitaet, Frankfurt, Germany

³ Forschungszentrum Karlsruhe, Institut fuer Kernphysik, Karlsruhe, Germany

⁴ Laboratoire SUBATECH, University of Nantes - IN2P3/CNRS - Ecole des Mines de Nantes, Nantes, France

Using the recently introduced model NEXUS 3, we calculate for pp , np and $\bar{p}p$ collisions the excitation function of particle yields and of average transverse momenta of different particle species as well as rapidity, x_F and transverse momentum distributions. Our results are compared with available data in between $\sqrt{s} = 5$ GeV and 65 GeV. We find for all observables quite nice agreement with data what make this model to a useful tool to study particle production in elementary hadronic reactions.

1 Introduction

The recently published Ω and $\bar{\Omega}$ data in pp collisions at 158 GeV by the NA49 collaboration have invalidated all customary quark-diquark string models [1, 2], which have been employed since long time to describe pp as well as AA collisions. In all those models, the valence quarks are taken as the end points of the strings, which provokes that due to the string topology [2] more $\bar{\Omega}$ than Ω are produced, in disagreement with the data. This effect has been verified in detailed calculations.

In the new NEXUS 3 model, the observed particles are produced by two sources: a) strings which are formed by sea (anti)quarks and which are therefore symmetric with respect to the exchange of a particle and an antiparticle and b) excited remnants, which decay statistically. Whereas

*Fellow of the Alexander von Humboldt Foundation

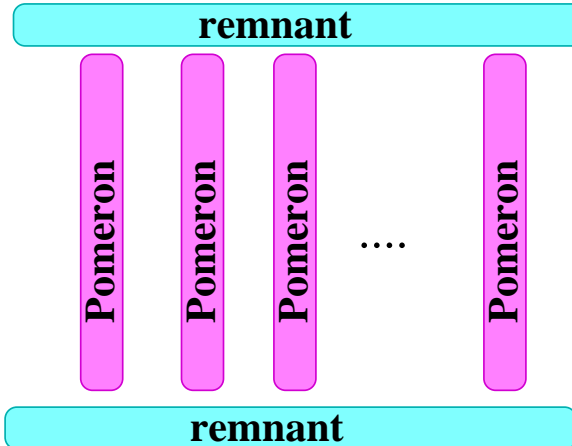


Figure 1: Multiple elementary interactions (Pomerons) in NEXUS .

the string produces an equal number of Ω and $\bar{\Omega}$, the remnant favors due to its finite baryon number the production of Ω , in accordance with the data.

In this paper, we calculate the results of the NEXUS 3 model for particle yields, rapidity distributions, transverse momentum distributions and average transverse momenta. Where experimental data are available we compare with them. We will show that the prediction of this model, once the necessary parameters are fixed to describe the CERN SPS pp data at 158 GeV and the excitation function of the multiplicity of charged particles, are in good agreement with the experimental data down to beam energies as low as 10 GeV . A similar, however less complete, comparison between data and string fragmentation models has recently be performed by H. Weber et al. [3]. They compare the URQMD and HSD model with data of nonstrange or single strange particles.

2 NEXUS 3

NEXUS 3 is a self-consistent multiple scattering approach to proton-proton and nucleus-nucleus scattering at high energies. The basic feature is the fact that several elementary interactions, referred to as Pomerons, may happen in parallel. We use the language of Gribov-Regge theory to calculate probabilities of collision configurations (characterized by the number of Pomerons involved, and their energy) and the language of strings to treat particle production.

We treat both aspects, probability calculations and particle production, in a consistent fashion: *In both cases energy sharing is considered in a rigorous way [4], and in both cases all Pomerons are identical.* This

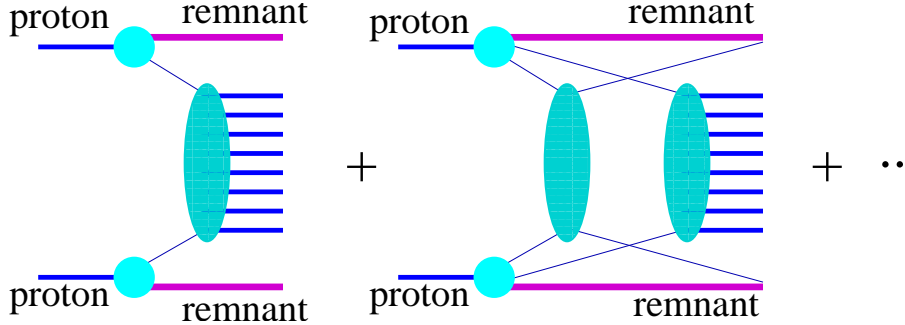


Figure 2: Inelastic scattering in pp . Partons from the projectile or the target proton interact via elementary interactions (the corresponding produced particles being represented by horizontal lines), leaving behind two remnants.

is one new feature of our approach. Another new aspect is the necessity to introduce remnants: The spectators of each baryon form a remnant, see Fig. 1. They will play an important role on particle production in the fragmentation region and at low energies ($E_{Lab} = 40\text{-}200 \text{ GeV}$). In the following we discuss some more details of our approach.

We first consider inelastic proton-proton scattering. We imagine an arbitrary number of elementary interactions to happen in parallel, where an interaction may be elastic or inelastic, see Fig. 2. The inelastic amplitude is the sum of all such contributions in which at least one inelastic elementary interaction is involved.

To calculate cross sections, we need to square the amplitude, which leads to many interference terms, as the one shown in Fig. 3(a), which represents interference between the first and the second diagram of Fig. 2. We use the usual convention to plot an amplitude to the left, and the complex conjugate of an amplitude to the right of some imaginary ‘‘cut line’’ (dashed vertical line). The left part of the diagram is a cut elementary diagram, conveniently plotted as a dashed line, see Fig. 3(b). The amplitude squared is now the sum over many such terms represented by solid and dashed lines.

When squaring the inelastic amplitude, all of the terms which correspond to the same final state interfere. For example, a single inelastic interaction does not interfere with a double inelastic interaction, whereas all the contributions with exactly one inelastic interaction interfere independent of the number of elastic collisions. So considering a squared amplitude, one may group terms together representing the same final state. In our pictorial language, this means that all diagrams with one dashed line, representing the same final state, may be considered to form a class, characterized by $m = 1 - \text{one dashed line}$ (one cut Pomeron) – and the light cone momenta x^+ and x^- attached to the dashed line (defining

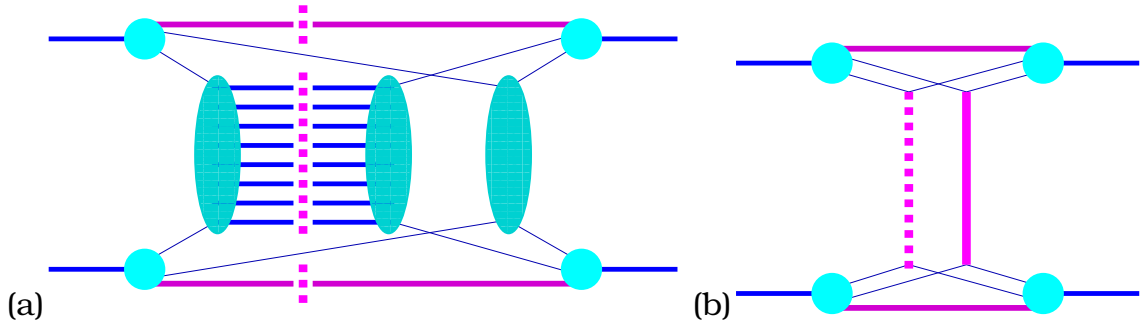


Figure 3: Inelastic scattering in pp . a) An interference term of cross section, b) Represented with our simplified notations.

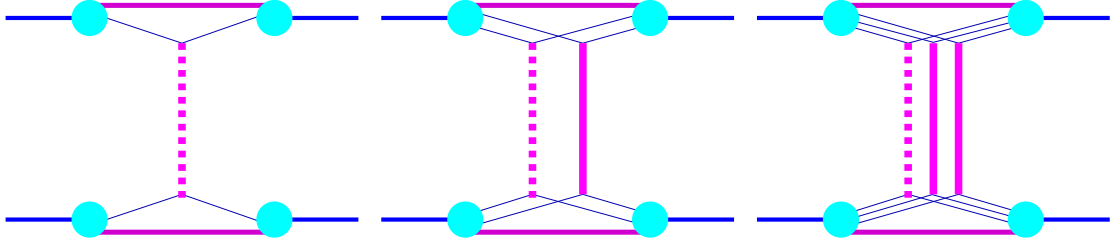


Figure 4: Class of terms corresponding to one inelastic interaction.

energy and momentum of the Pomeron). In Fig. 4, we show several diagrams belonging to this class, in Fig. 5, we show the diagrams belonging to the class of two inelastic interactions, characterized by $m = 2$ and four light-cone momenta $x_1^+, x_1^-, x_2^+, x_2^-$.

Generalizing these considerations, we may group all contributions with m inelastic interactions. The sum of all these terms represents the probability of having m inelastic interactions with $x_1^+ \dots x_{2m}^+$, $x_1^- \dots x_{2m}^-$ at a given impact parameter. Integrating over impact parameter provides the corresponding cross section. By this we obtain a probability distribution for the number of elementary interactions (number of Pomerons) and the momenta of these Pomerons.

How to form strings from Pomerons? No matter whether single-Pomeron

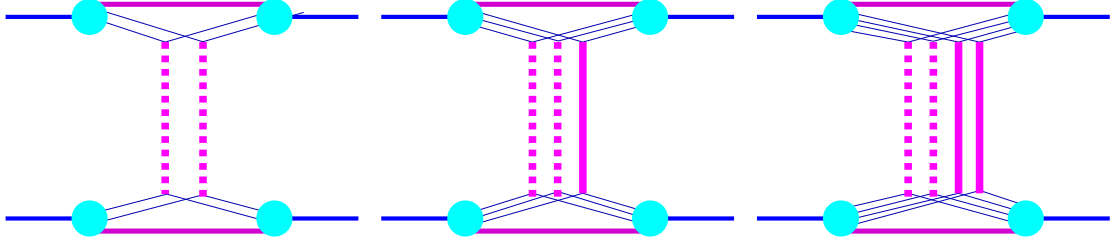


Figure 5: Class of terms corresponding to two inelastic interactions.

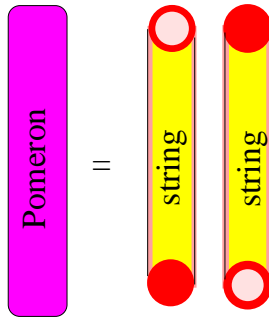


Figure 6: Each Pomeron is identified with two strings.

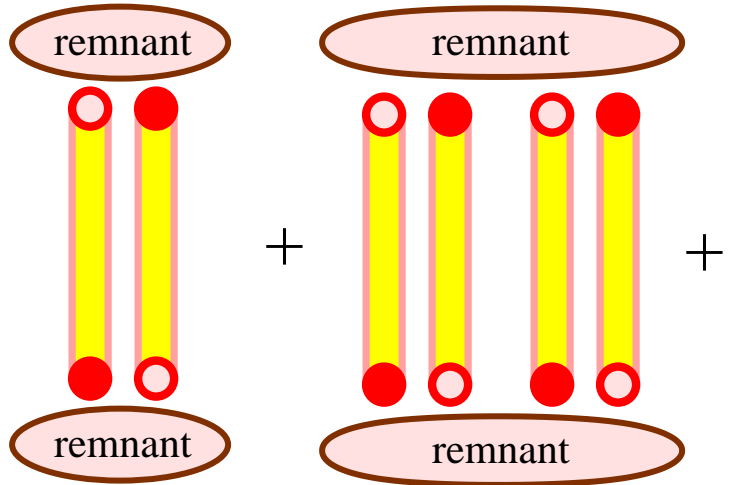


Figure 7: Remnants in single (two strings) and double scattering (four strings): in any case, two remnants contribute.

or multiple-Pomeron exchange happens in a proton-proton scattering, all Pomerons are treated identically. Each Pomeron is identified with two strings, see Fig. 6.

The string ends are quarks and antiquarks from the sea. This differs from traditional string models, where all the string ends are valence quarks. Due to the possibility of having a large number of Pomerons, this is impossible in our approach. The valence quarks stay in remnants. Being formed from sea quarks, string ends from cut Pomerons have complete flavour symmetry and produce particles and antiparticles in equal amounts.

Remnants are new objects, compared to other string models, see Fig. 7. The partonic content of a remnant is as follows: three valence quarks and the corresponding antiparticles of the partons representing the string ends. The masses of remnants are assumed to be small compared to the kinetic energies involved and are therefore neglected for the calculations

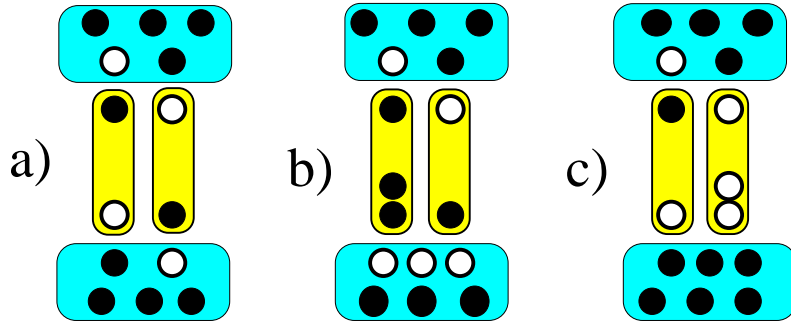


Figure 8: a) The most simple and frequent collision configuration has two remnants and only one cut Pomeron represented by two $q - \bar{q}$ strings. b) One of the \bar{q} string-ends can be replaced by a qq string-end. c) With the same probability, one of the q string-ends can be replaced by a $\bar{q}\bar{q}$ string-end.

of multi-Pomeron configurations. To obtain finally the masses, one parameterizes the mass distribution of a remnant as $P(m^2) \propto (m^2)^{-\alpha}$, $m^2 \in (m_{\min}^2, x^+ s)$, where s is the squared energy at center mass system, m_{\min} is the minimum mass of hadrons to be made from the remnant's quarks and antiquarks, and x^+ is the light-cone momentum fraction of the remnant which is determined in the collision configuration. Through fitting the data at 158 GeV we determine the parameter $\alpha = 1.5$. Remnants decay into hadrons according to n-body phase space[5].

The leading order and therefore the most simple and most frequent collision configuration has two remnants and only one cut Pomeron represented by two $q - \bar{q}$ strings as in Fig. 8a. Besides the three valence quarks, each remnant has additionally a quark and an antiquark to compensate the flavour.

In NEXUS 3, this most simple approach is slightly modified by allowing with a small probability P_{qq} that an antiquark \bar{q} at one of the legs of the Pomeron is replaced by a diquark qq . The corresponding string ends are then a diquark and a quark. In this way we get quark-diquark ($q - qq$) strings from cut Pomerons. The qqq Pomeron end has to be compensated by the three corresponding antiquarks in the remnant, as in Fig. 8b. The $(3q3\bar{q})$ remnant may decay into three mesons (3M) or a baryon and an anti-baryon ($B + \bar{B}$), but the 3M mode is favored by phase space. For symmetry reasons, the q leg of a cut Pomeron is replaced by an antidiquark $\bar{q}\bar{q}$ with the same probability P_{qq} . This yields a $\bar{q} - \bar{q}\bar{q}$ string and a $(6q)$ remnant, as shown in Fig. 8c. The $(6q)$ remnant decays into two baryons. Since $q - qq$ strings and $\bar{q} - \bar{q}\bar{q}$ strings have the same probability to appear from cut Pomerons, baryons and antibaryons are produced in the string fragmentation with the same probability. However, from remnant decay, baryon production is favored due to the initial valence quarks.

With decreasing energy, the relative importance for the particle production of the strings decreases as compared to the remnants, because the energy of the string is lowered as well. If the mass of the string is lower than the cut off, it will be discarded. However, the fact that an interaction has taken place is taken into account by the excitation of the remnant which follows still the above mentioned distribution.

3 Results

To fix the main parameters for the Pomerons and the strings, we use the total cross section for pp scattering, the excitation functions for all identified charged particle yields from $\text{sqrt}(s)=10 \text{ GeV}$ to 2 TeV and the rapidity, p_t and multiplicity distributions for at 200 GeV lab and cms and 1800 GeV for charged particles. To adjust the parameters of the remnant decay and the multistrange baryon production, we mainly use the NA49 results at 158 GeV lab. Then, with this set of parameters, we compare the simulation results to all pp data at quite wide energy range and also to np data at beam energy 40 GeV . This comparison work is not trivial, firstly because with decreasing beam energy the importance of the remnants for the particle production increases as compared to the pomerons. Secondly, pp collisions fix only the sum of the contributions of remnants and pomerons which contribute to different rapidity regions. The comparison of the predictions for np collisions with data reveals whether each individual source of particle production is correctly described.

3.1 Hadron Multiplicities

3.1.1 Energy Dependence of Average Multiplicities

We start our investigation with the 4π multiplicities at different energies. In fig. 9 we display the excitation function of charged particles [7]-[25] as compared to the NEXUS 3 results. The Λ $\bar{\Lambda}$ and K_S have been identified and their decay products are not included here. The agreement between calculation and experiment shows that this approach is able to describe excitation functions.

Now we come to the excitation function of identified hadrons. The predictions for 4π multiplicities of identified hadrons are shown in figs. 10, 11, 12 and here as well we find agreement with most of the data over a wide energy range, from $\sqrt{s} = 5 \text{ GeV}$ to 63 GeV . The largest discrepancies we observe for the ϕ meson and for the \bar{p} at low energies. It would be interesting to see in which rapidity region this discrepancies appears (especially because the $\bar{\Lambda}$ is reasonable well reproduced but unfortunately

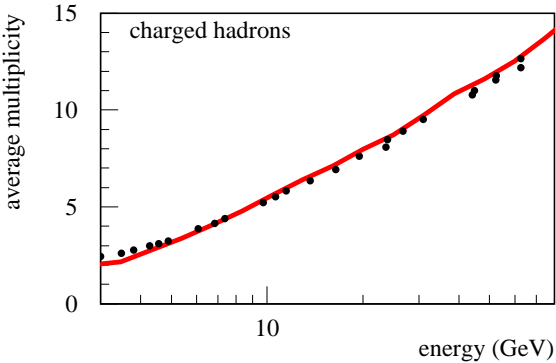


Figure 9: Excitation function of charged particle [7]-[25] as compared to the NEXUS results. The Λ , $\bar{\Lambda}$ and K_S have been identified and their decay products are not included.

such data are not available.

3.1.2 K/π ratios

Special interest has recently gained the excitation function of the K/π ratio because it has been claimed that the appearance of a maximum in the K^+/π^+ excitation function, observed in heavy ion reactions, may be a signature that the plasma of quarks and gluons is formed. Although we are not concerned with heavy ion reactions here we display these ratios for later reference in fig. 13. Neither data nor calculation show a maximum of the K^+/π^+ ratio in this elementary collision.

3.1.3 Rapidity Spectra

We come now to more detailed information by studying the rapidity distribution. Fig. 14 shows the rapidity distribution of a multitude of hadrons for the reaction 40 GeV pp. Where data from the NA49 collaboration are available we have included them in the plot. The numbers give the average multiplicity of the hadrons in 4π . We see that the experimental data are reasonably well described. The non-strange baryons as well as those which contain one strange quark show a double hump structure, the others are peaked at midrapidity. This is a consequence of the three source structure (two remnants and Pomerons) in our approach. The leading baryon has still the quantum number of the incoming baryon but is moderately excited. Therefore it may disintegrate into baryons whose quantum numbers differ not too much. Also the calculation of the np reaction at 40 GeV, displayed in Fig. 15, reproduces the data quite nicely. We see of course a much lower number of protons in the fragmentation

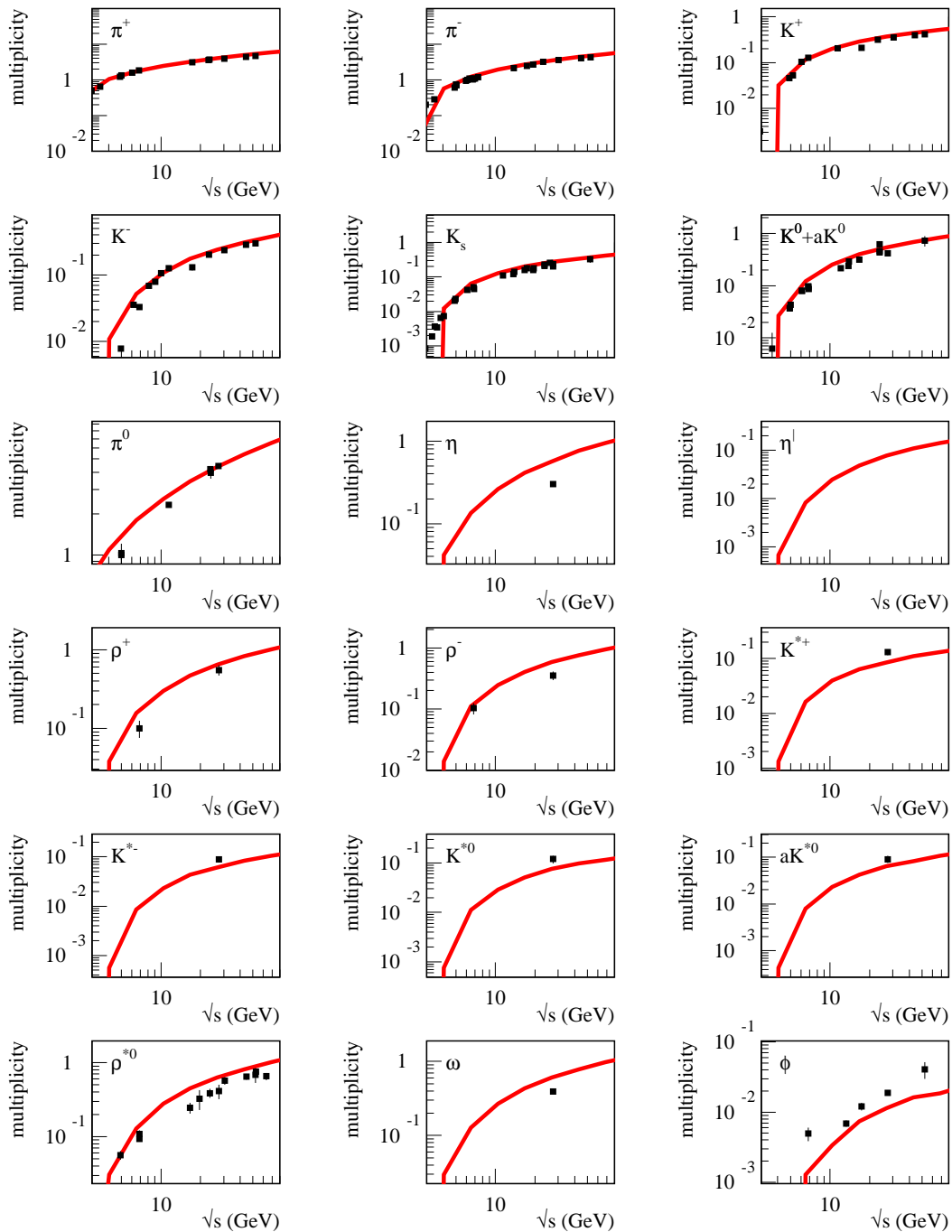


Figure 10: Excitation function of the multiplicity of identified hadrons as compared with the available data (squares) [7]-[50].

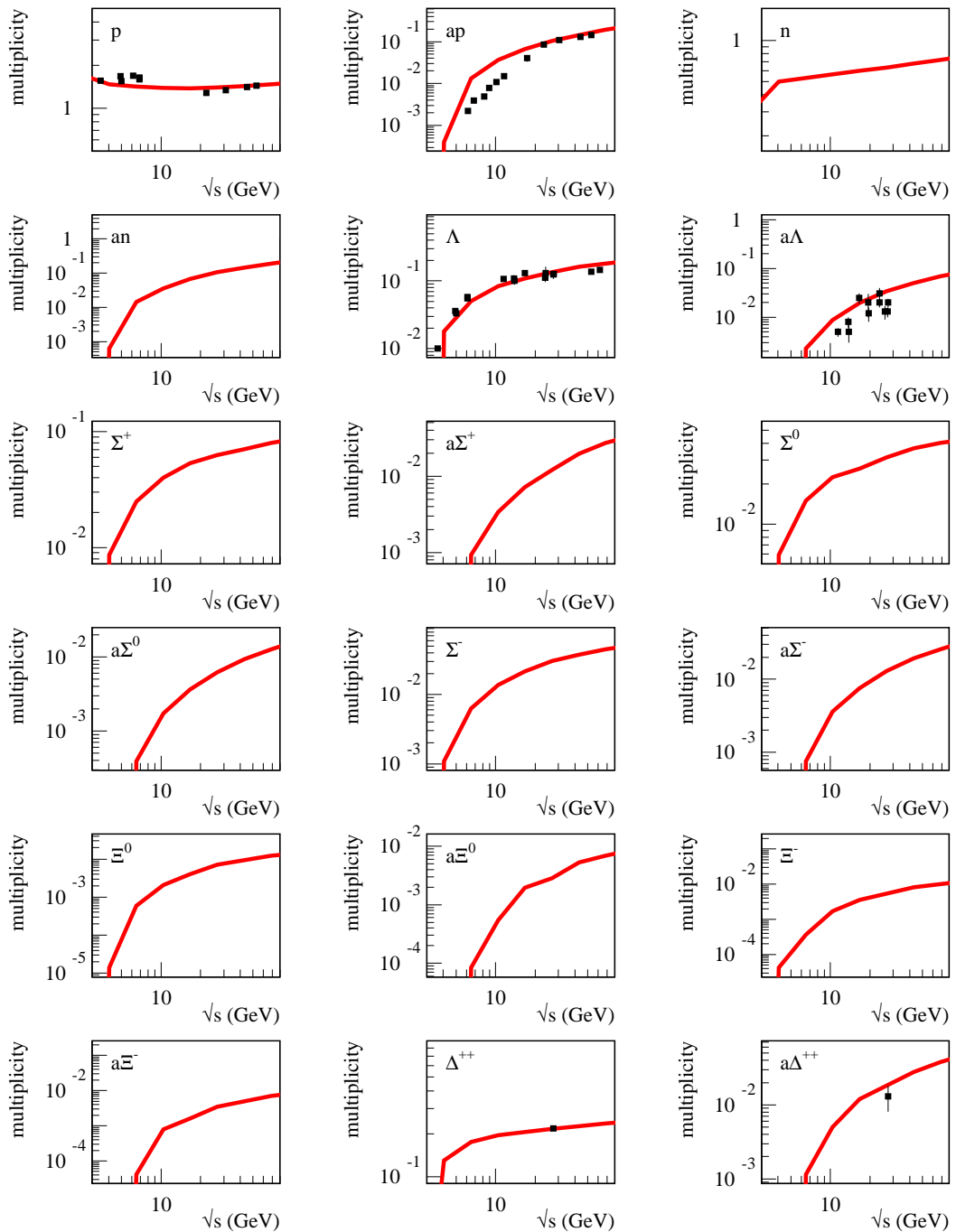


Figure 11: The same as Fig. 10.

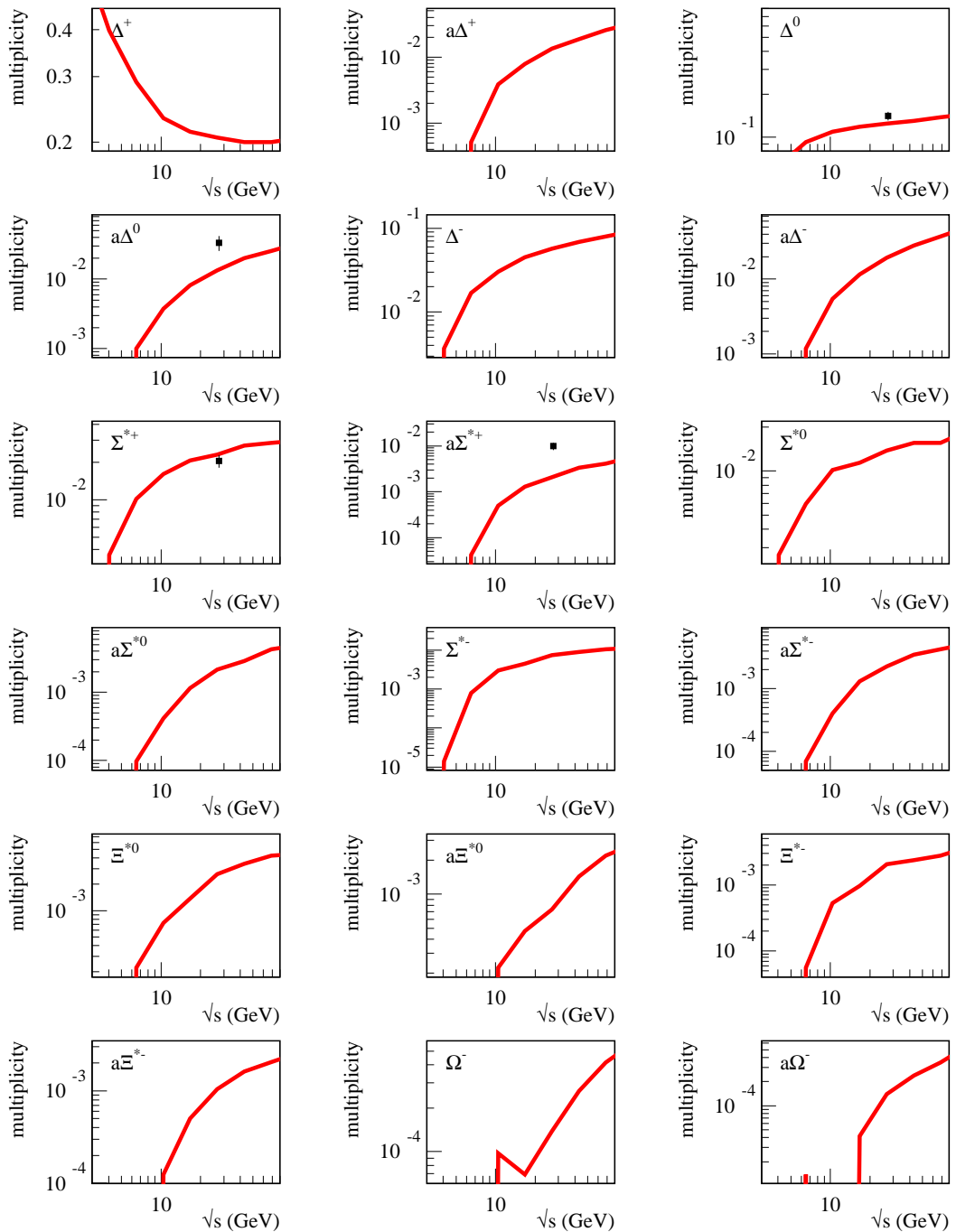


Figure 12: The same as Fig. 10.

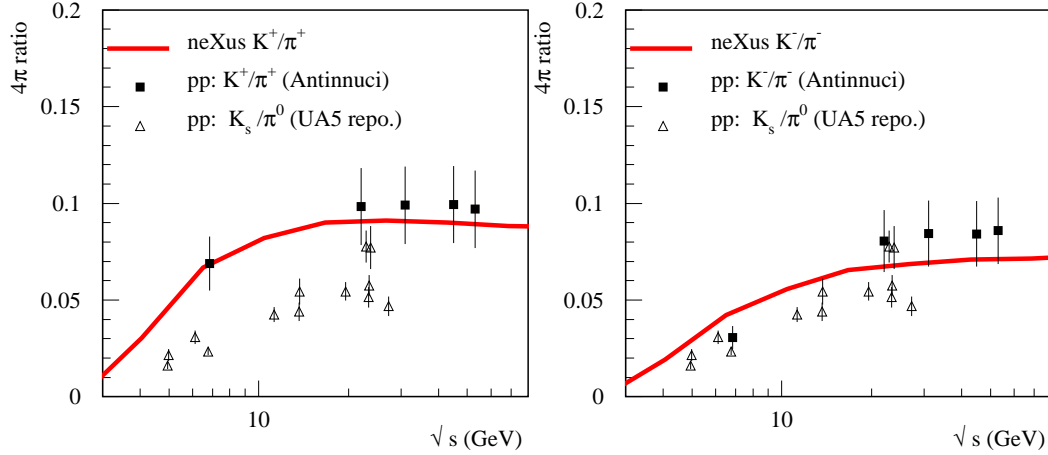


Figure 13: Theoretical and experimental K/π ratio. Squared points are from [45], triangle points represent the K_s/π_0 ratio and are from [26]-[44], compiled in [7].

region. This difference to the pp collision is well reproduced. This agreement validates the correct description of the basic mechanism for particle production in the fragmentation region. A comparison between the spectra shows that the difference between pp and np in the pion spectra extends to negative rapidities (as seen as well in the data). For Λ and $\bar{\Lambda}$ as well as for the other charge zero particles, the difference between pp and np is negligible. Naturally $\Sigma^+(\Sigma^-)$ are more copiously produced if the projectile is a p(n).

Fig. 16 shows the rapidity spectra for pp at 100 GeV. Again we see a quite reasonable agreement between data and calculation. At 158 GeV, Fig. 17, we included the experimental Λ , $\bar{\Lambda}$, Ξ , $\bar{\Xi}$ spectra which have recently been published [1]. We observe also more Ω than $\bar{\Omega}$ as seen in experiment [6]. This is a consequence of the modification of NEXUS 3 explained in [1] as compared to the original NEXUS 2 version [4] which yields more $\bar{\Omega}$ than Ω due to the string topology .

For ISR energies there are only rapidity distributions for a given transverse momentum. In figs. 18 and 19 we display for $p_T = 0.4$ GeV/c the rapidity distributions for π^+ , π^- , K^+ , K^- , p , \bar{p} for energies in between $E_{cm} = 23$ GeV and 63 GeV. We see that also here the spectra agree well with the data where data are available.

Fig. 20 shows the longitudinal x_F distributions of identified hadrons from pp collisions at a beam energy 400 GeV. In order to be comparable with the before-mentioned rapidity distributions, we use a logarithmic representation of the x-axis. We see that also here the spectra agree reasonably well with the LEBC-EHS Col. data[50]. Please note that there

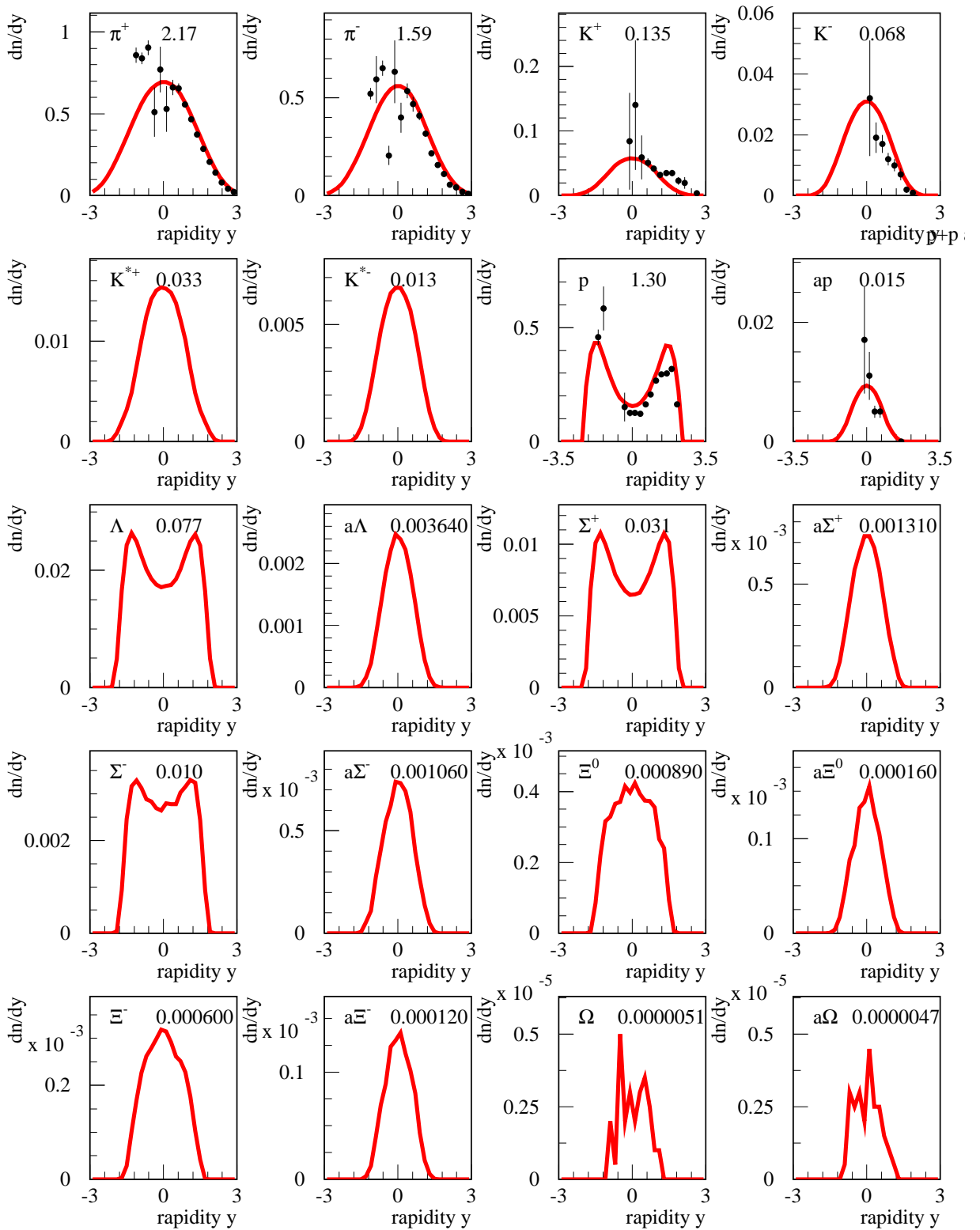


Figure 14: Rapidity spectra (lines) and 4π multiplicities (numbers) of identified hadrons from proton-proton at beam energy 40 GeV. Data are from [6].

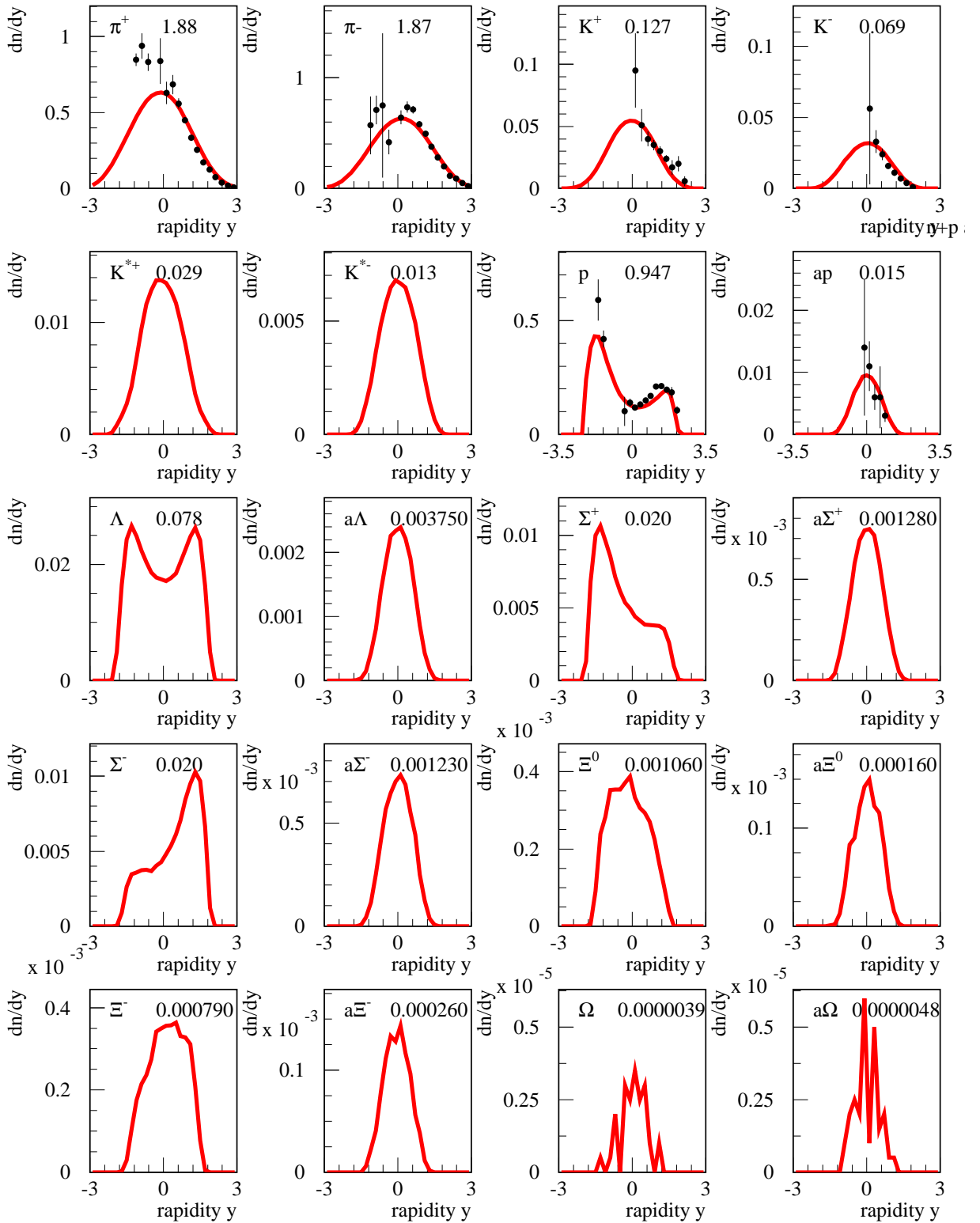


Figure 15: Rapidity distribution (lines) and 4π multiplicities (numbers) of identified hadrons for neutron-proton collisions at a beam energy of 40 GeV. Data are from [6].

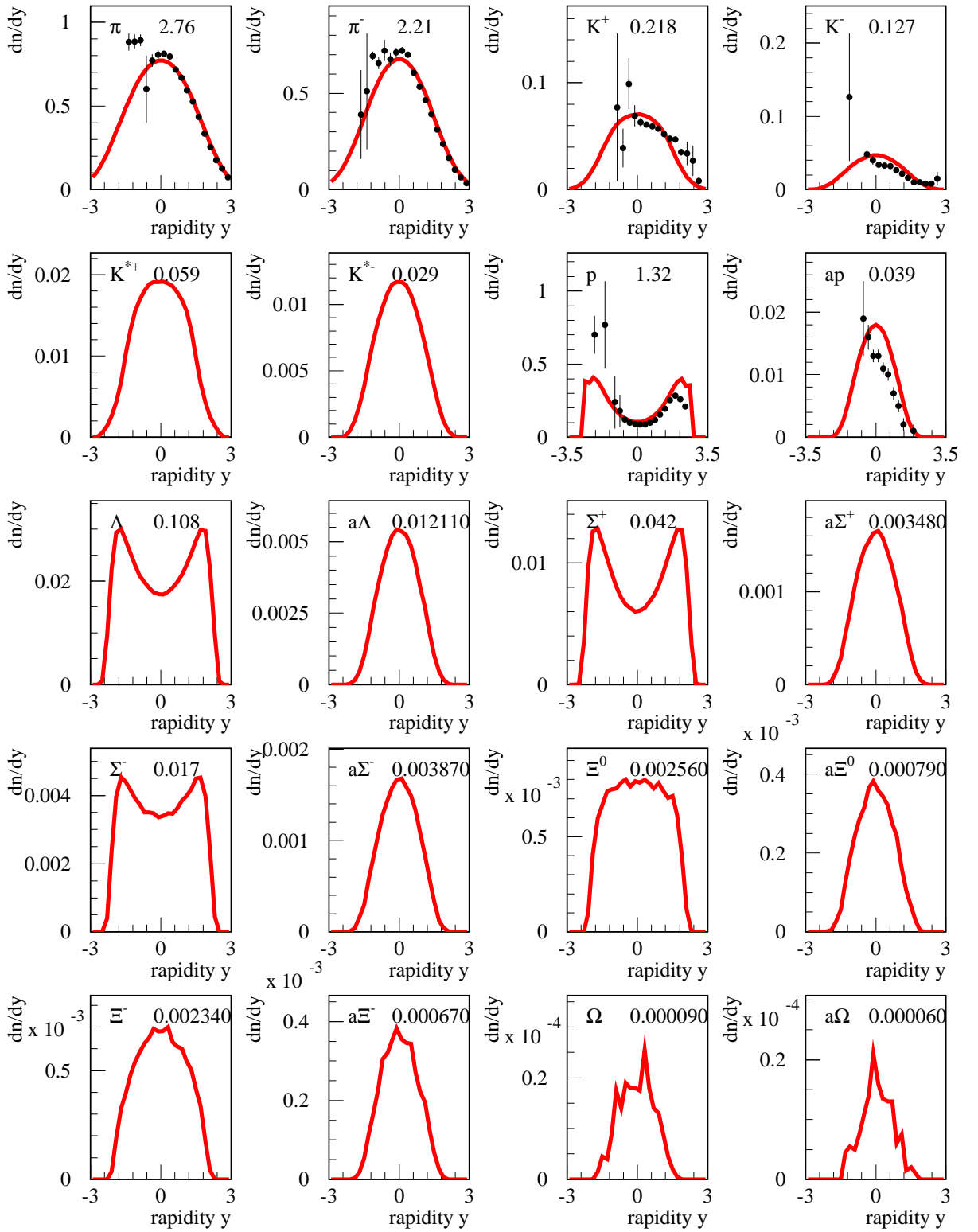


Figure 16: Rapidity distribution (lines) and 4π multiplicities (numbers) of identified hadrons for proton-proton collisions at a beam energy of 100 GeV. Data are from [6].

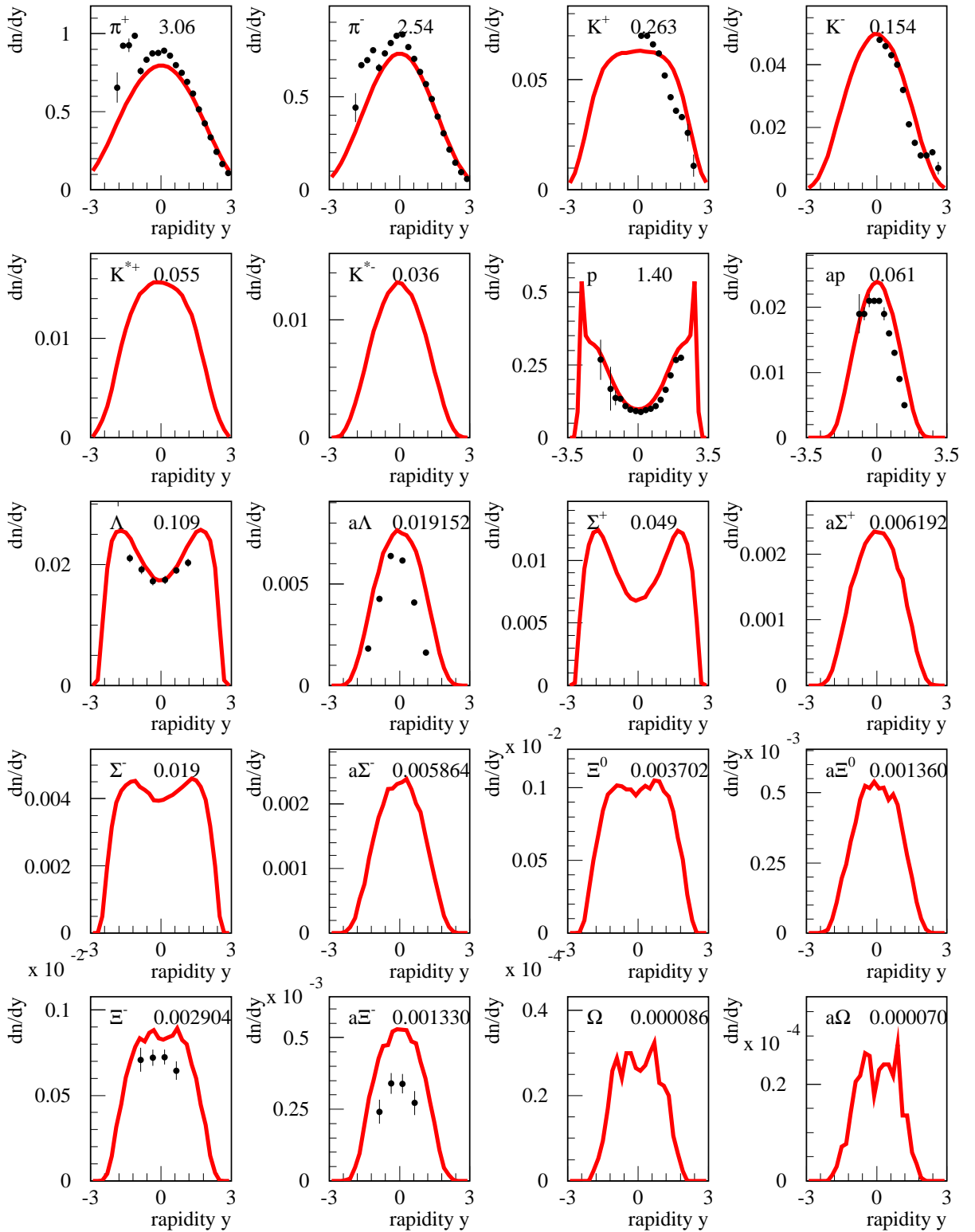


Figure 17: Rapidity distribution (lines) and 4π multiplicities (numbers) of identified hadrons for proton-proton collisions at a beam energy of 158 GeV. Data are from [6].

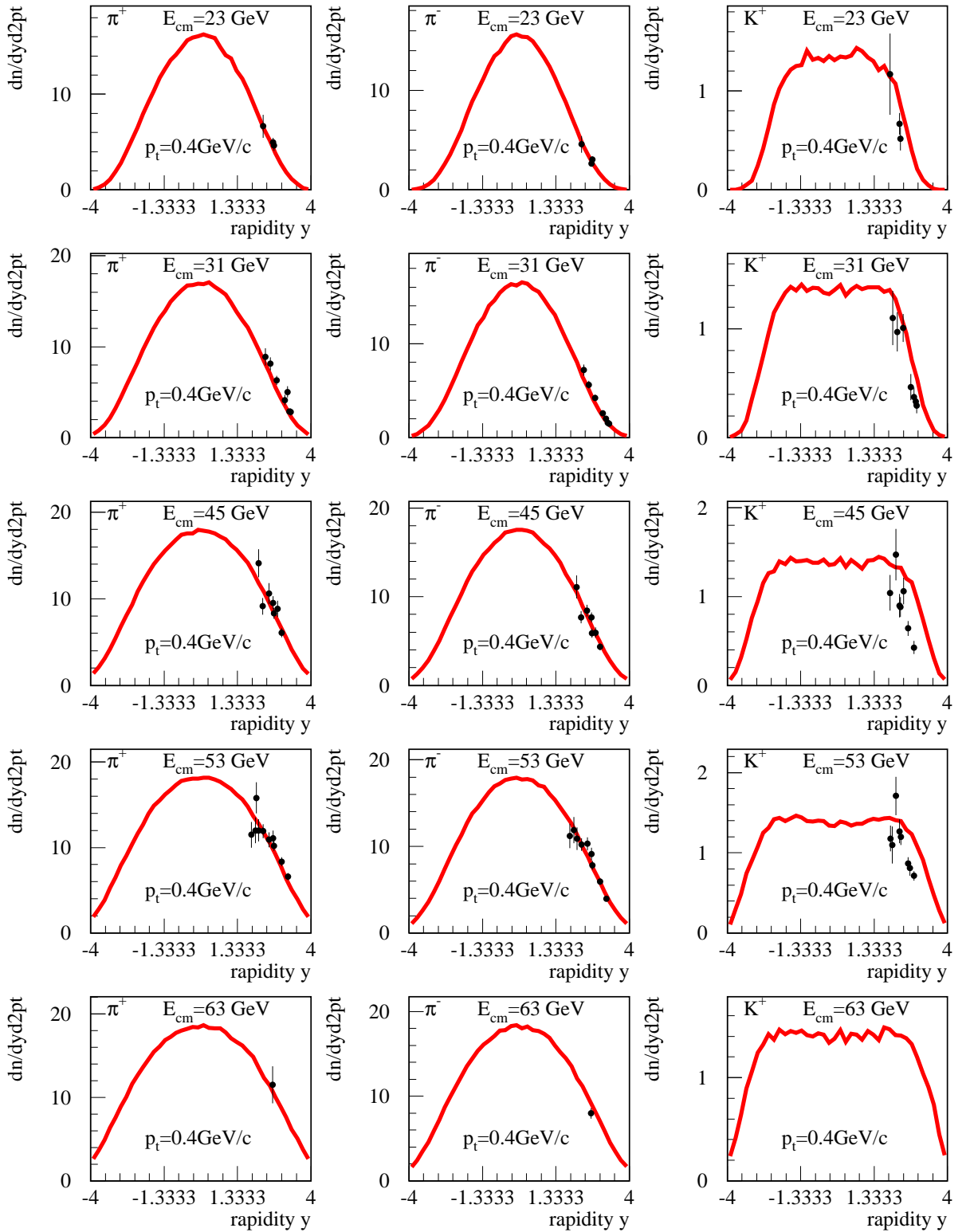


Figure 18: π^+ , π^- and K^+ rapidity distributions at $p_t=0.4\text{GeV}/c$ for proton-proton collisions at ISR energies. Data are from [53].

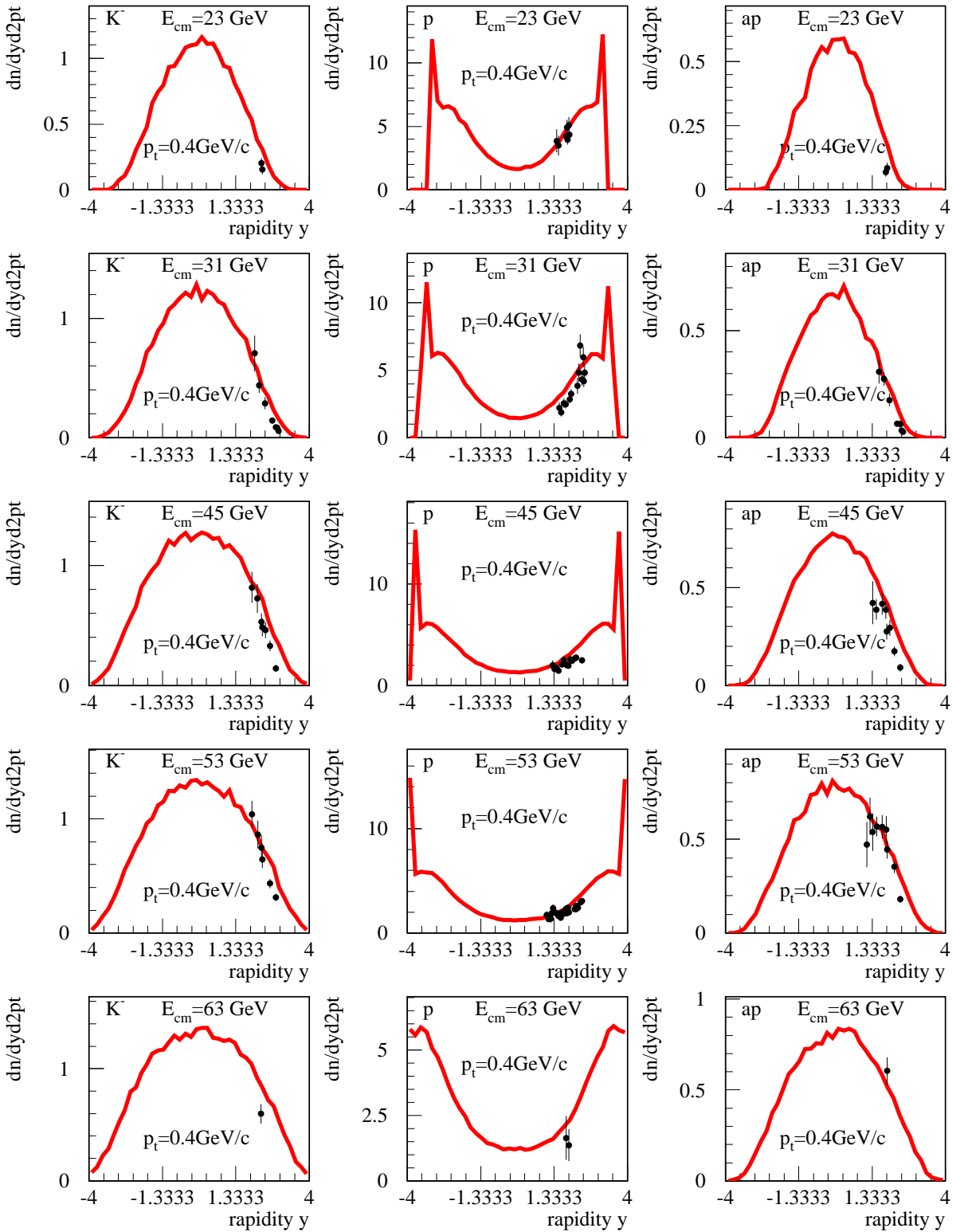


Figure 19: K^- , proton and antiproton rapidity distributions at $p_t=0.4\text{GeV}/c$ for proton-proton collisions at ISR energies. Data are from [53].

are two curves for the ρ 's. This is due to the inconsistency of the two available data sets: $x_E dn/dx_F$ and dn/dx_F spectra. So dn/dx_F spectra from our simulations are additionally plotted as dashed lines there.

3.2 Transverse Momentum

3.2.1 Average Transverse Momenta

Fig. 21 displays the excitation function of the average transverse momentum for all charged particles and several particle species in comparison with the experimental data[51]. We see that with the exception of K^+ , the average transverse momentum is reproduced over the whole kinematical range. For the K^+ we underpredict the average transverse momentum at smaller beam energies.

3.2.2 Transverse Momentum Distribution

At SPS energies not only the mean transverse momenta but also the whole transverse momentum spectra is available and we compare these data with the NEXUS 3 predictions in figs. 22,23,24. Again, the agreement is quite reasonable up to $p_t = 2\text{GeV}$. The calculation of the spectra at higher transverse momenta at SPS energies is beyond the limits of present day computers, because of the very small cross section of hard process.

4 Conclusions

Employing the recently developed NEXUS **3** model where the parameters have been mainly fixed to the pp data at $E_{lab} = 158\text{ GeV}$, we compare its predictions on average quantities, longitudinal and transverse spectra between $\sqrt{s} = 5\text{ GeV}$ and 65 GeV with the existing data of pp , np and $\bar{p}p$ collisions.

We find a very nice agreement with data for 4π multiplicities, rapidity and x_F distributions as well as for transverse momenta. This suggests that the basic mechanism of particle production is well described in the NEXUS **3** model. Based on this observation we can use this model to study pA and AA collisions which will be the subject of a forthcoming publication.

References

- [1] F.M. Liu, J. Aichelin, M. Bleicher, H.J. Drescher, S. Ostapchenko, T. Pierog, K. Werner, Phys. Rev. D **67** (2003) 034011;

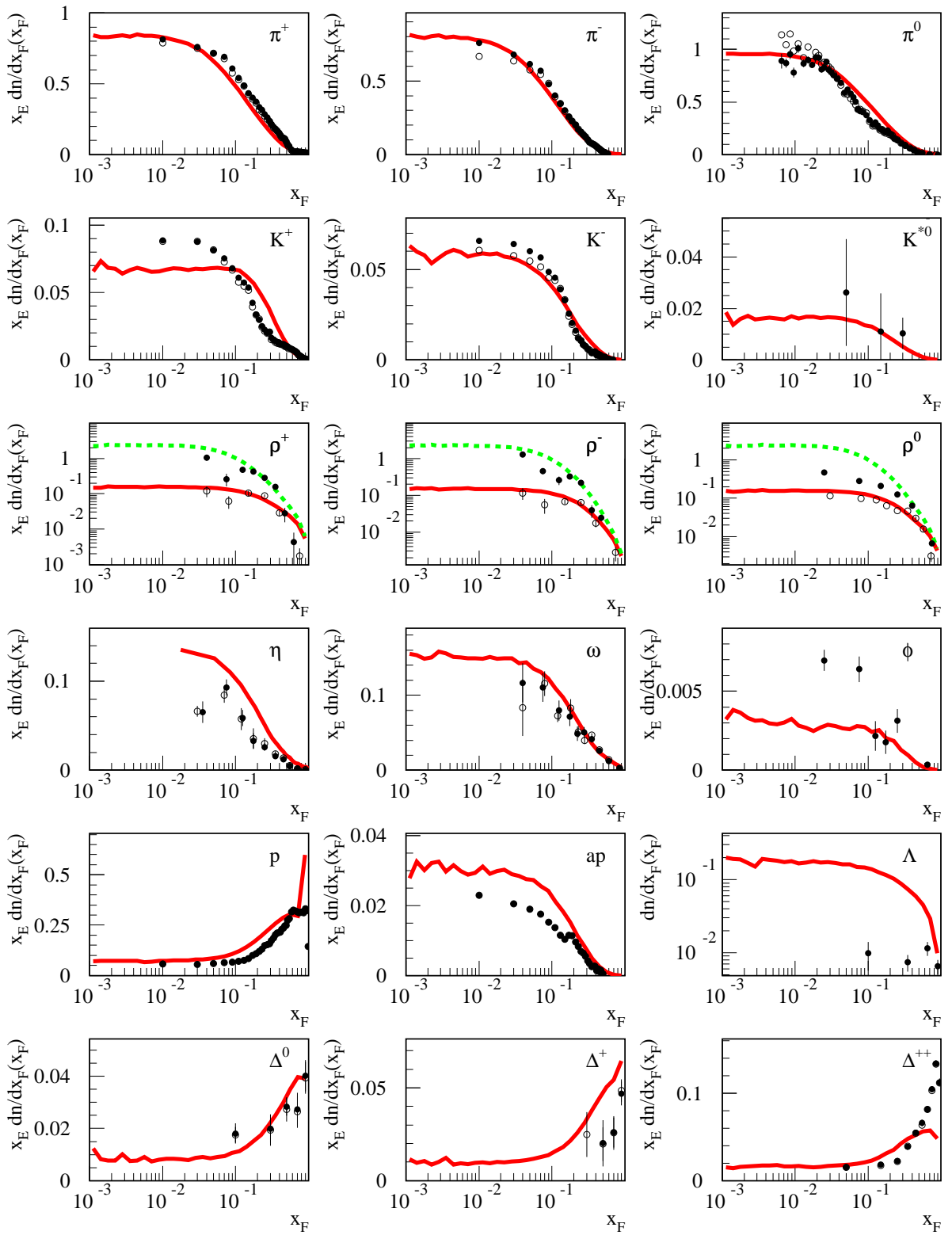


Figure 20: x_F distributions of identified hadrons from pp collisions at beam energy 400 GeV. Data are from [50]. The vertical axis of dashed lines and the points in rho meson plots is dn/dx_F .

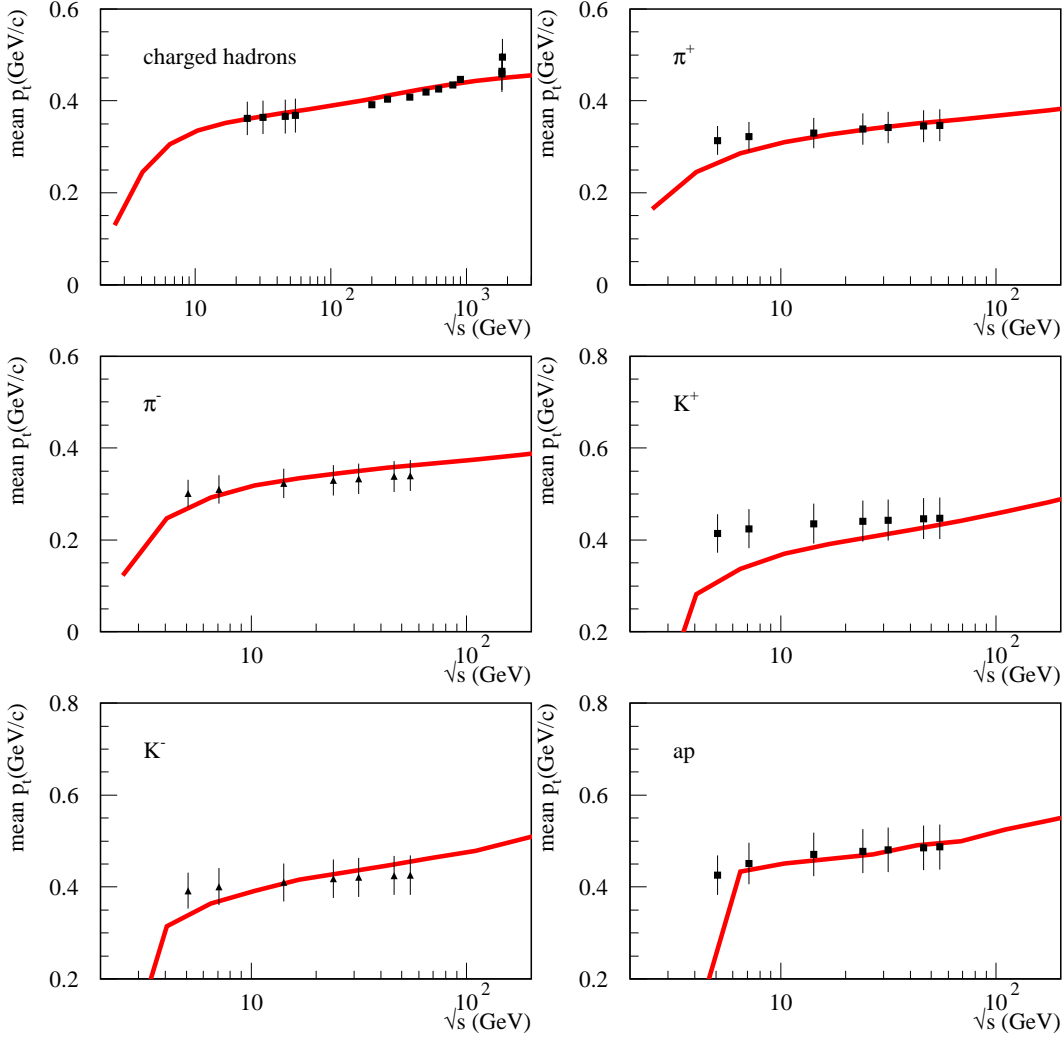


Figure 21: Average transverse momentum of charged hadrons, pions, kaons and antiproton from 4π phase space at different energies. Data are from [51].

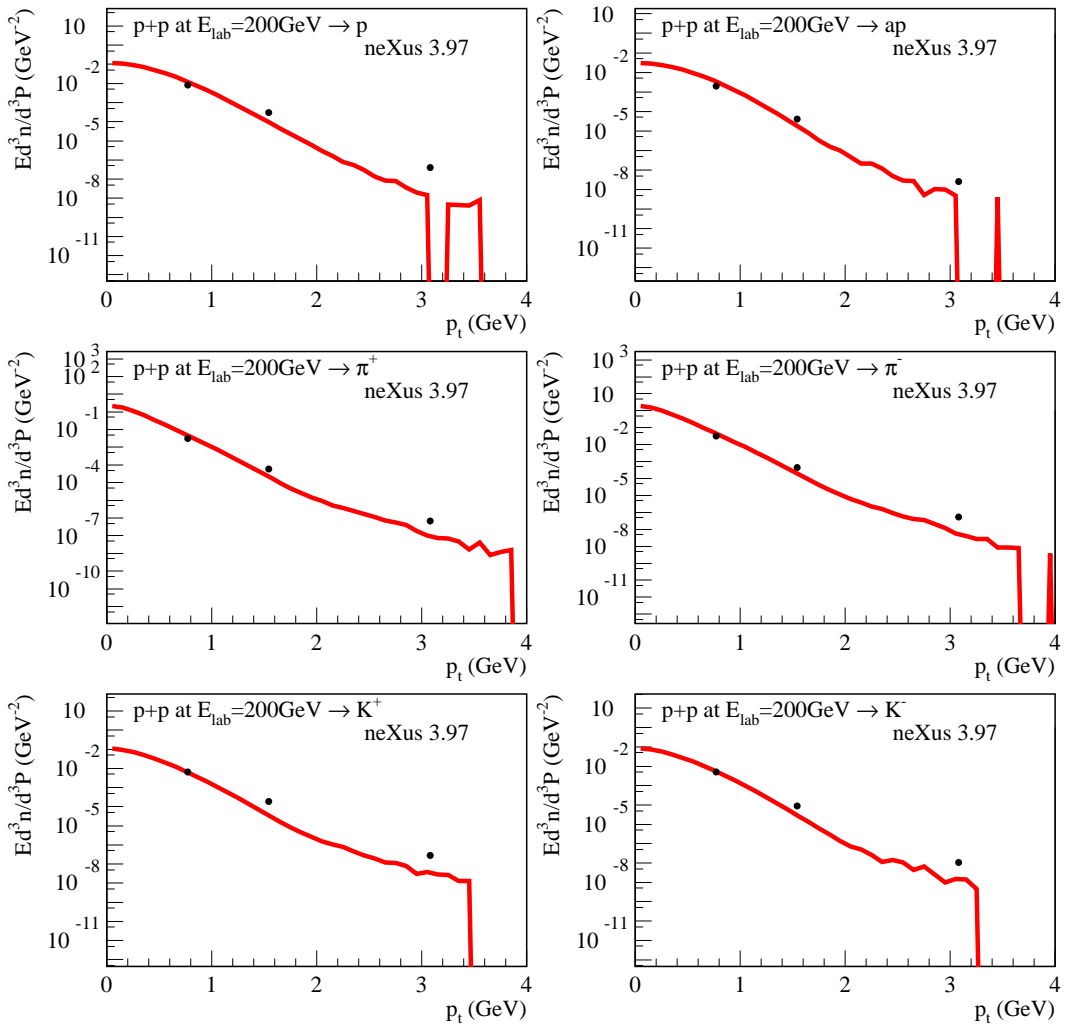


Figure 22: Transverse momentum spectra of proton, antiproton, charged pions and Kaons from pp collisions at $E_{\text{lab}} = 200 \text{ GeV}$. Data are from [52].

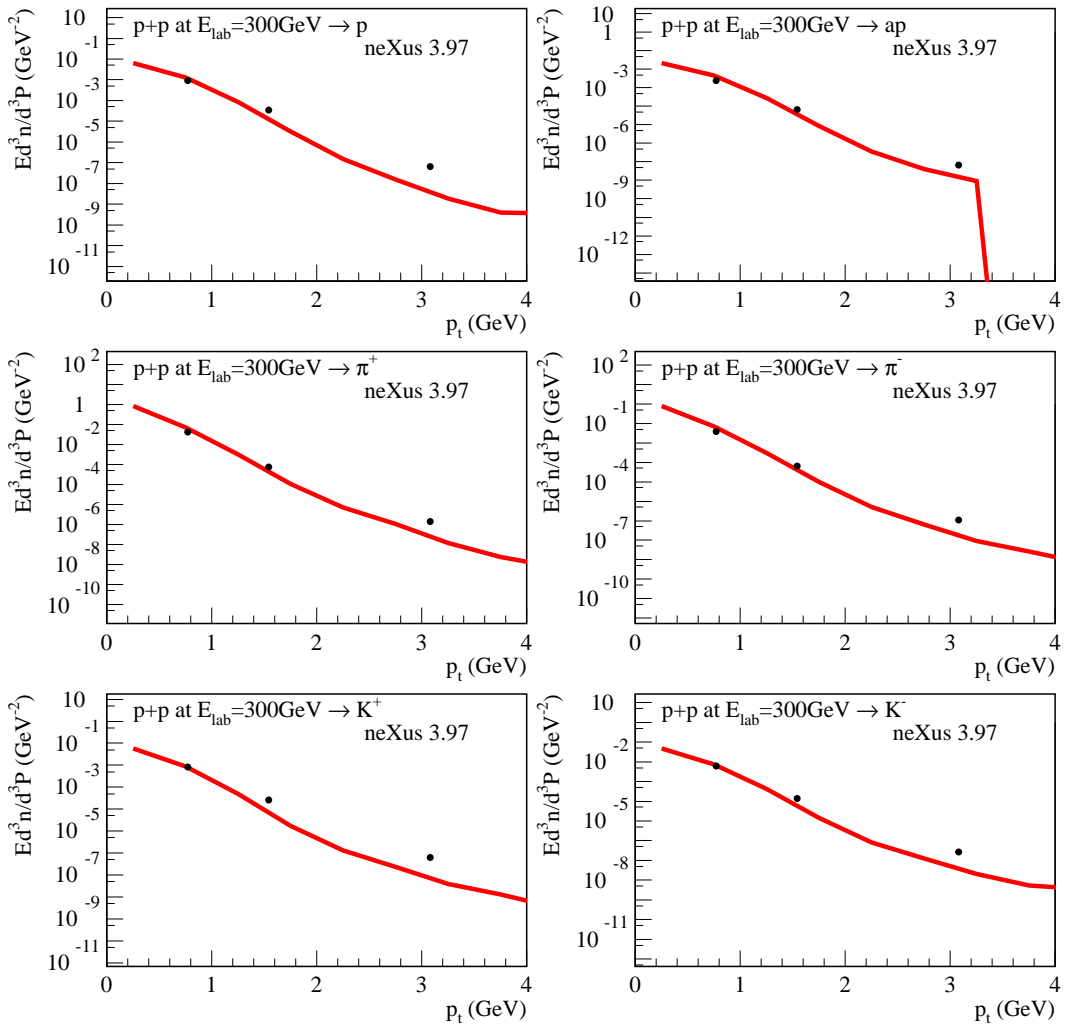


Figure 23: Transverse momentum spectra of proton, antiproton, charged pions and Kaons from pp collisions at $E_{\text{lab}} = 300\text{GeV}$. Data are from [52].

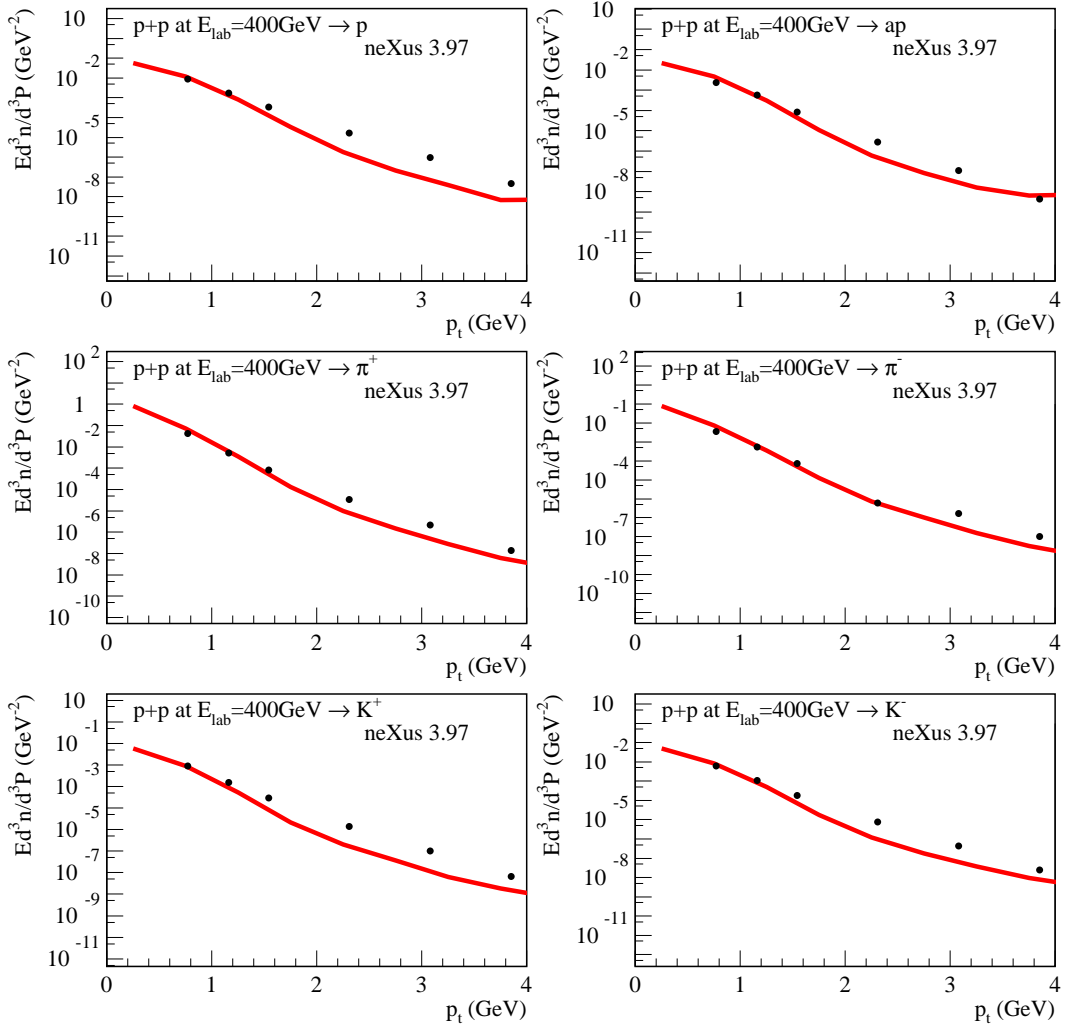


Figure 24: Transverse momentum spectra of proton, antiproton, charged pions and Kaons from pp collisions at $E_{\text{lab}} = 400 \text{ GeV}$. Data are from [52].

- F.M. Liu, K. Werner, talk for PASI 2002, Campos do Jordao, Brazil, 7-18 Jan 2002, AIP Conf. Proc. **631** (2003) 422.
- [2] M. Bleicher, F. M. Liu, A. Keränen, J. Aichelin, S.A. Bass, F. Becattini, K. Redlich, K. Werner, Phys. Rev. Lett. **88** (2002) 202501.
 - [3] H. Weber, E. L. Bratkovskaya, W. Cassing and H. Stoecker, Phys. Rev. C **67** (2003) 014904.
 - [4] H.J. Drescher, M. Hladik, S. Ostapchenko, T. Pierog, K. Werner, Phys. Rept. **350** (2001) 93.
 - [5] K. Werner and J. Aichelin, Phys. Rev. C **52** (1995) 1584
 - [6] NA49 collaboration, Addendum-10 to Proposal CERN/SPSC/P264, 'Progress Report and Beam Request for 2002';
Hadron in nuclear collisions NA49 collaboration, homepage;
T. Susa for NA49 collaboration, Nucl. Phys. A **698** (2002) 491;
M. V. Leeuwen for NA49 collaboration, Nucl. Phys. A **715** (2003) 161;
M. Mitrovski for NA49 collaboration, nucl-ex/0305029.
 - [7] G. J. Alner *et al.* [UA5 Collaboration], Phys. Rept. **154** (1987) 247.
 - [8] V. V. Ammosov *et al.*, Phys. Lett. B **42** (1972) 519.
 - [9] W. M. Morse *et al.*, Phys. Rev. D **15** (1977) 66.
 - [10] S. Barish *et al.*, Phys. Rev. D **9** (1974) 2689.
 - [11] A. Firestone *et al.*, Phys. Rev. D **10** (1974) 2080.
 - [12] C. Bromberg *et al.*, Phys. Rev. Lett. **31** (1973) 1563.
 - [13] A. Breakstone *et al.* [Ames-Bologna-CERN-Dortmund-Heidelberg-Warsaw Collaboration], Phys. Rev. D **30** (1984) 528.
 - [14] G.A. Smith *et al.*, Phys. Rev. Lett. **123** (1961) 2160;
E.L. Hart *et al.*, Phys. Rev. Lett. **126** (1962) 747.
 - [15] L. Bodini *et al.*, Nuovo Cim. A **58** (1968) 475;
S. Coletti *et al.*, Nuovo Cim. A **49** (1967) 479.
 - [16] C. Alexander *et al.*, Phys. Rev. **154** (1967) 1284.
 - [17] G. Yekutieli *et al.*, Nucl. Phys. B **18** (1970) 301. S. Danieli, A. Shapira, Y. Eisenberg, B. Haber, E. E. Ronat, G. Yekutieli and J. Grunhaus, Nucl. Phys. B **27** (1971) 157.

- [18] C. n. Booth *et al.*, Phys. Rev. D **27** (1983) 2018.
- [19] S. P. Almeida *et al.*, Phys. Rev. **174** (1968) 1638.
- [20] V. Blobel *et al.* [Bonn-Hamburg-Munich Collaboration], Nucl. Phys. B **69** (1974) 454.
- [21] H. Boeggild *et al.*, Nucl. Phys. B **27** (1971) 285.
- [22] W. H. Sims, J. Hanlon, E. O. Salant, R. S. Panvini, R. R. Kinsey, T. W. Morris and L. Von Lindern, Nucl. Phys. B **41** (1972) 317.
- [23] C. Bromberg, T. Ferbel, T. Jensen and P. Slattery, Phys. Rev. D **15** (1977) 64.
- [24] D. Brick *et al.*, Phys. Rev. D **25**, 2794 (1982).
- [25] W. Thome *et al.* [Aachen-CERN-Heidelberg-Munich Collaboration], Nucl. Phys. B **129** (1977) 365.
- [26] K. Jaeger *et al.*, Phys. Rev. D **11** (1975) 1756.
- [27] M. Alston-Garnjost, J. Erwin, J. H. Klems, W. Ko, R. L. Lander, D. E. Pellett and P. M. Yager, Phys. Rev. Lett. **35** (1975) 142.
- [28] J. W. Chapman *et al.*, Phys. Lett. B **47** (1973) 465.
- [29] K. Jaeger, D. Colley, L. Hyman and J. Rest, Phys. Rev. D **11** (1975) 2405.
- [30] A. Sheng *et al.*, Phys. Rev. D **11** (1975) 1733.
- [31] R. D. Kass *et al.*, Phys. Rev. D **20** (1979) 605.
- [32] R. L. Eisner *et al.*, Nucl. Phys. B **123** (1977) 361.
- [33] B. Y. Oh and G. A. Smith, Nucl. Phys. B **49** (1972) 13.
- [34] K. Alpgard *et al.* [Scandinavian Bubble Chamber Collaboration], Nucl. Phys. B **103** (1976) 234.
- [35] J. Bartke *et al.*, Nuovo Cim. **29** (1963) 8.
- [36] V. V. Ammosov *et al.*, Nucl. Phys. B **115** (1976) 269.
- [37] D. Brick *et al.*, Nucl. Phys. B **164** (1980) 1.
- [38] F. Lopinto *et al.*, Phys. Rev. D **22** (1980) 573.
- [39] F. T. Dao *et al.*, Phys. Rev. Lett. **30** (1973) 1151.

- [40] M. Asai *et al.* [EHS-RCBC Collaboration], Z. Phys. C **27** (1985) 11.
- [41] H. Kichimi *et al.*, Phys. Rev. D **20** (1979) 37.
- [42] A. M. Rossi, G. Vannini, A. Bussiere, E. Albini, D. D'Alessandro and G. Giacomelli, Nucl. Phys. B **84** (1975) 269.
- [43] D. Drijard *et al.*, Z. Phys. C **9** (1981) 293.
- [44] D. Drijard *et al.* [CERN-Dortmund-Heidelberg-Warsaw Collaboration], Z. Phys. C **12** (1982) 217.
- [45] M. Antinucci *et al.*, Lett. Nuovo Cim. **6** (1973) 121.
- [46] M. Banner *et al.* [UA2 Collaboration], Phys. Lett. B **122** (1983) 322.
- [47] R.E. Ansorge *et al.*, Nucl. Phys. B **328** (1989) 36.
- [48] M. Gazdzicki and D. Rohrich, Z. Phys. C **71** (1996) 55 [arXiv:hep-ex/9607004].
- [49] J. Bachler *et al.* (NA49 Collaboration), Nucl. Phys. A **661** (1999) 45; S.V. Afanasev *et al.* (NA49 Collaboration), Phys. Lett. B **491** (2000) 59.
- [50] M. Aguilar-Benitez *et al.*, LEBC-MPS Collaboration, Z. Phys. C **50** (1991) 405.
- [51] Rossi *et al.*, Nucl. Phys. B **84** (1975) 269-305; C. Albajar *et al.* (UA1 collaboration), Nucl. Phys. B **335** (1990) 261-287.
- [52] Antreasyan *et al.*, Phys. Rev. D **19** (1979) 764; Antreasyan *et al.*, Phys. Rev. Lett. **38** (1977) 112.
- [53] Capiluppi *et al.*, Nucl. Phys. B **79** (1974) 187.

